

3D-QSAR and molecular docking studies of 1,3,5-triazene-2,4-diamine derivatives against r-RNA: Novel bacterial translation inhibitors

Y. Nataraja Sekhar^a, M. Ravi Shashi Nayana^b, N. Sivakumari^a,
Muttineni Ravikumar^{b,*}, S.K. Mahmood^a

^a Bioinformatics division, Environmental Microbiology Lab, Department of Botany, Osmania University, Hyderabad 500007, AP, India

^b Biocampus, S-1, Phase-1, Technocrats Industrial Estate, Balanagar, Hyderabad 500037, AP, India

Received 24 September 2007; received in revised form 12 January 2008; accepted 23 January 2008

Available online 12 February 2008

Abstract

Aminoglycoside mimetics inhibit bacterial translation by interfering with the ribosomal decoding site. To elucidate the structural properties of these compounds important for antibacterial activity, comparative molecular field analysis (CoMFA) and comparative molecular similarity indices analysis (CoMSIA) were applied to a set of 56 aminoglycosides mimetics. The successful CoMFA model yielded the leave-one-out (LOO) cross-validated correlation coefficient (q^2) of 0.708 and a non-cross-validated correlation coefficient (r^2) of 0.967. CoMSIA model gave $q^2 = 0.556$ and $r^2 = 0.935$. The CoMFA and CoMSIA models were validated with 36 test set compounds and showed a good r^2_{pred} of 0.624 and 0.640, respectively. Contour maps of the two QSAR approaches show that electronic effects dominantly determine the binding affinities. These obtained results were agreed well with the experimental observations and docking studies. The results not only lead to a better understanding of structural requirements of bacterial translation inhibitors but also can help in the design of novel bacterial translation inhibitors.

© 2008 Elsevier Inc. All rights reserved.

Keywords: QSAR; CoMFA; CoMSIA; Docking; Antibiotics; Translation inhibitors; 1,3,5-Triazine-2,4-diamine derivatives; r-RNA

1. Introduction

Most of the infections are caused by a wide range of bacteria, resulting in mild to life-threatening illnesses that require immediate intervention. The fight against bacterial infection represents one of the high points of modern medicine. The development of bacterial resistance to existing drugs is a major problem in antibacterial therapy and necessitates continuing research into new classes of anti bacteria [1]. Major challenge in antibiotic discovery is to develop compounds with broad-spectrum activity especially for infections caused by multidrug-resistant Gram-positive pathogens. The recent and rapid spread of community acquired methicillin-resistant *Staphylococcus aureus* (MRSA) [2–4] also giving rise to linezolid-resistant MRSA strains [5]. To overcome the bacterial resistance, ribosome is the proven drug target against diverse bacterial groups. Many of the clinically important antibiotic classes

including macrolides, tetracyclines, aminoglycosides and oxazolidinones bind to this target. Aminoglycosides are currently the best characterized class of small molecules that interact specifically with RNA [6]. This represents a macro-molecule class that has largely been ignored in target driven drug discovery programs [7–9]. Recently, a set of potent 1,3,5-triazine-2,4-diamine derivatives (TDA) (Fig. 1) were prepared, similar to aminoglycoside compounds [10–12]. These novel aminoglycoside mimetics inhibit bacterial translation, presumably by interfering with the ribosomal decoding site (A-site) [10].

The present study aimed at elucidating the structural features of 1,3,5-triazine-2,4-diamine derivatives required for bacterial translation inhibition and to obtain predictive three-dimensional quantitative structure activity relationship (3D-QSAR) model, which may guide the rational synthesis of novel inhibitors. In this paper, we report the 3D-QSAR model derived using comparative molecular field analysis (CoMFA) [13] and comparative molecular similarity indices analysis (CoMSIA) [14] for TDA derivatives as antibacterial translation inhibitors. The generated 3D-QSAR models would give insight to the

* Corresponding author. Tel.: +91 9989899074.

E-mail address: ravambio@gmail.com (M. Ravikumar).

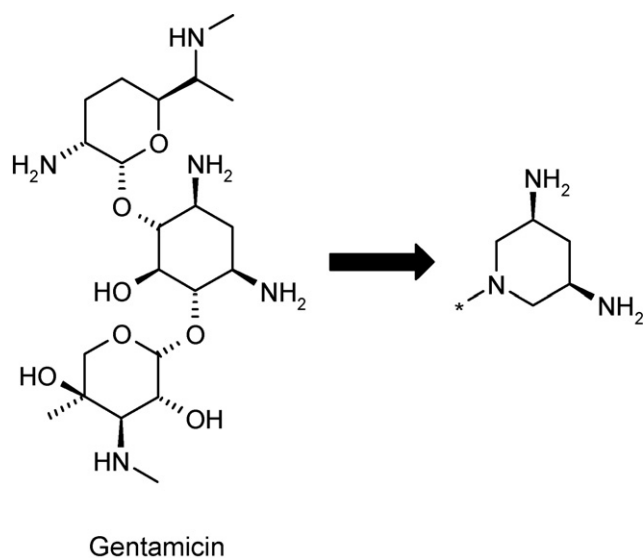


Fig. 1. The aminoglycoside gentamicin and the TDA scaffold that mimics 2-deoxystreptamine of the aminoglycoside.

influence of various interactive fields on the activity and thus, can help in designing and forecasting the translation inhibition activity of novel molecules. Further, docking studies are also performed to analyze the interactions between ribonucleic acid (RNA) and ligand, which will be helpful in designing of novel antibacterial compounds.

2. Methods

2.1. Data set and molecular modeling

A data set of 92 potent 1,3,5-triazine-2,4-diamine derivatives (TDA), reported to have antibacterial translation inhibitory activities were used for the following QSAR and Docking studies (Table 1) [10–12]. The data set and biological data of compounds were taken from literature, evaluated by similar group. The total set of inhibitors was divided into a training set (55 compounds) for generating 3D QSAR models and a test set (37 compounds) for validating the quality of the models. Selection of the training set and test set molecules was done based on the structural diversity and wide range of activity such that the test set molecules represent a range of biological activity similar to that of the training set; thus, the test set is truly representative of the training set. *In vitro* inhibitory concentrations (IC_{50}) of the molecules were converted into corresponding pIC_{50} (Table 1) and used as dependent variables in the 3D QSAR calculations.

All the molecular modeling studies were performed using SYBYL 6.8.1 [15] on silicon graphics workstation. Initially, one of the most active compounds **63** (since it is having higher similarity with most of the compounds used in the model generation) was sketched. Minimization of this compound was performed in SYBYL using Tripos force field [16] and Gasteiger [17] charges with a convergence criterion of 0.005 kcal/mol. Conformational search was performed using systematic search. Systematic search explores conformational

space in a regular and predictable fashion by rotating the flexible bond, systematically from 0° to 360° by incrementing 30° of step size. Each conformer generated was minimized and the lowest energy conformer was considered for further geometric optimization using the semi-empirical AM1 Hamiltonian [18] of MOPAC 6 package, since it is a semi-empirical method and more accurate than molecular mechanics. The optimized conformation was docked in to the t-RNA to predict the biologically active conformation. The docked conformation was used as a template to sketch rest of the molecules.

2.2. Alignment procedure

In general, a geometric similarity should exist between the modeled structures and that of the bioactive conformation for 3D QSAR. The spatial alignment of compounds under study is thus one of the most sensitive and determining factors in obtaining a reliable model. Hence, we have used the docked conformation of compound **63** as a template and sketched remaining molecules. These conformations were aligned to generate the predictive QSAR model. The molecular alignment was carried out using the atom-based rms fit method with ALIGN DATABASE command available in SYBYL. This option uses alignment of structures through pair-wise atom super positioning places all structures in the database in the same frame of reference as the template compound. The most active compound, **63** was used as template and the remaining molecules were aligned to it through using the basic core of 1,3,5-triazine. The aligned molecules are shown in Fig. 2.

2.3. CoMFA calculations

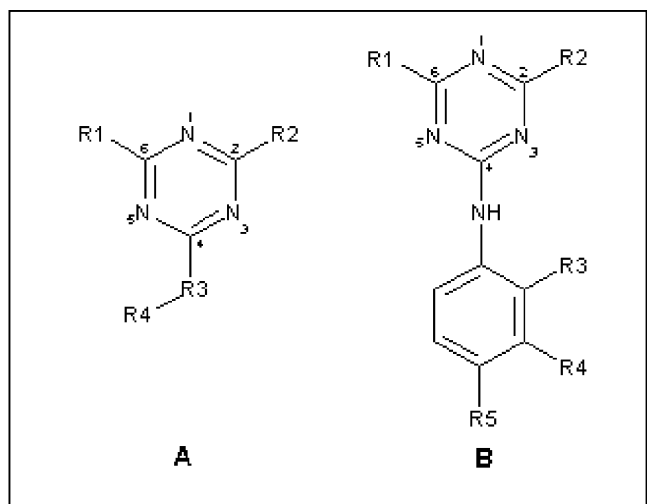
The steric and electrostatic CoMFA potential fields were calculated at each lattice intersection of a regularly spaced grid of 2.0 Å in x , y and z direction using Lennard–Jones potential for steric fields and columbic terms for electrostatic fields. The grid box dimensions were determined automatically in such a way that the region boundaries were extended beyond 4 Å in each direction from the co-ordinates of each molecule. A distance dependent dielectric constant of 1.0 was used, sp^3 hybridized carbon atom with +1 charge served as probe atom to calculate steric and electrostatic fields. The steric and electrostatic contributions were truncated to 30.0 kcal/mol. CoMFA quantifies the interaction energy between a probe molecule in the molecular field and a set of aligned target molecules in a QSAR. Interaction energies measured and analyzed for a set of 3D structures can be useful in establishing QSAR.

2.4. CoMSIA calculations

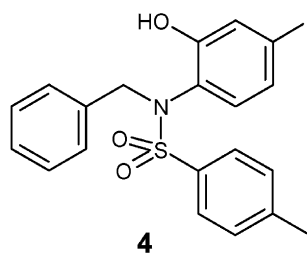
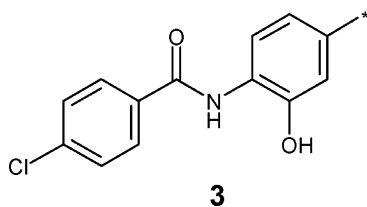
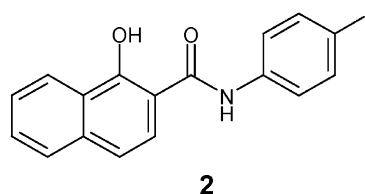
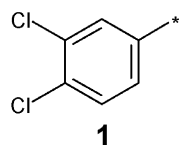
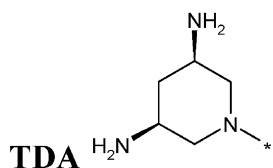
CoMSIA computes the steric and electrostatic fields (as in CoMFA), but it also calculates additional hydrophobic, hydrogen-bond donor and hydrogen-bond acceptor fields. The resulting contour maps are easier to interpret than those in CoMFA because a Gaussian function is used to determine the distance-dependence. Therefore, the similarity indices can also

Table 1

Structures and biological data of 1,3,5-triazine-2,4-diamines (TDA) used to derive Co MFA and CoMSIA models [10–12]



Side Groups



Comp.	S	R1	R2	R3	R4	R5	IC ₅₀ (μM)	pIC ₅₀
1	A			Cl	---	---	42	4.377
2	A	TDA	TDA	NH ₂	---	---	92	4.036
3	A	TDA	TDA	NHOH	---	---	45	4.347
4	A	TDA	TDA	NHCH ₃	---	---	62	4.208
5	A	TDA	TDA	NHNH ₂	---	---	170	3.769
6	A	TDA	TDA	N(CH ₃) ₂	---	---	290	3.538
7	A	TDA	TDA		---	---	180	3.745
8	A	TDA	TDA			---	63	4.201
9*	A	TDA	TDA		-	---	23	4.638
10	A	TDA	TDA			---	36	4.444
11*	A	TDA	TDA			---	32	4.495

Table 1 (Continued)

12	A	TDA	TDA			---	9	5.046
13	A	TDA	TDA			---	7	5.155
14	A	TDA	TDA			---	8	5.097
15	A	TDA	TDA			---	4	5.398
16	A	TDA	TDA			---	4	5.398
17*	A	TDA	TDA			---	3	5.523
18*	A	TDA	TDA			---	5	5.301
19	A	TDA	TDA			---	5	5.301
20	A	TDA	TDA			---	4	5.398
21	A	TDA	TDA			---	13	4.886
22*	A	TDA	TDA			---	15	4.824
23	A	TDA	TDA			---	11	4.959
24*	A	TDA	TDA			---	14	4.854
25	A	TDA	TDA			---	11	4.959
26	B	TDA	TDA	H	OMe		8	5.097
27*	B	TDA	TDA		OMe	H	30	4.523
28	B	TDA	TDA	H	H		5	5.301
29*	B	TDA	TDA	H		H	4	5.398
30	A	TDA	TDA			---	9	5.046
31	A	TDA	TDA			---	7	5.156

Table 1 (Continued)

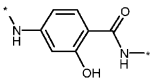
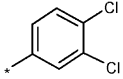
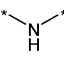
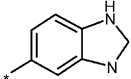
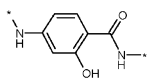
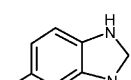
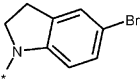
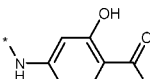
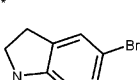
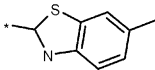
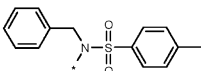
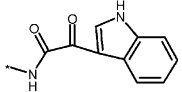
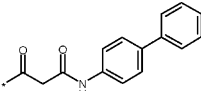
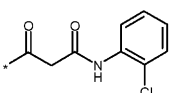
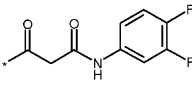
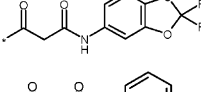
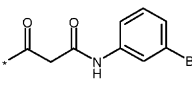
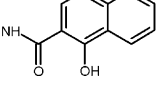
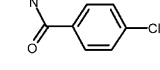
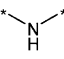
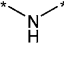
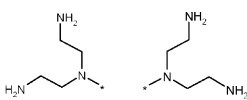
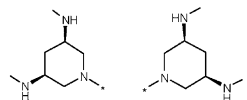
32	A	TDA	TDA			---	10	5
33	A	TDA	TDA			---	14	4.854
34	A	TDA	TDA			---	4	5.398
35	A	TDA	TDA	-		---	5	5.301
36*	A	TDA	TDA			---	9	5.046
37*	B	TDA	TDA	H	H		10	5
38	B	TDA	TDA	H	OH		4	5.398
39	B	TDA	TDA	H	OH		4	5.398
40	B	TDA	TDA	H	H		6	5.222
41	B	TDA	TDA	H	H		4	5.398
42*	B	TDA	TDA	H	H		9	5.046
43*	B	TDA	TDA	H	H		6	5.222
44	B	TDA	TDA	H	H		5	5.301
45	B	TDA	TDA	H	H		10	5
46	B	TDA	TDA	H	OH		7	5.155
47	A	TDA	TDA		1	---	10	5
48*	A	TDA	TDA		2	---	7	5.155
49	A				2	---	7	5.155
50	A				1	---	5	5.301

Table 1 (Continued)

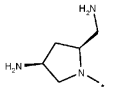
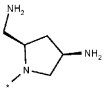
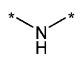
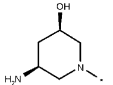
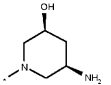
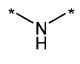
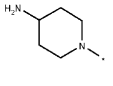
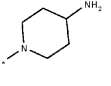
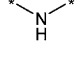
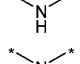
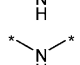
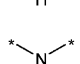
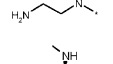
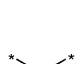
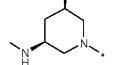
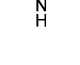
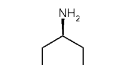
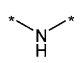
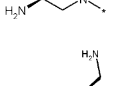

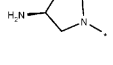

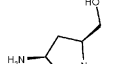
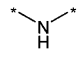
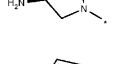

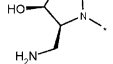
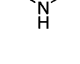
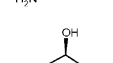
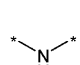
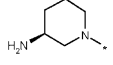
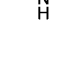
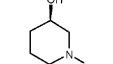
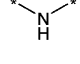
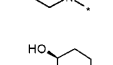
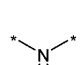
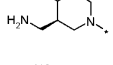
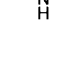
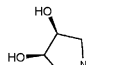
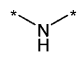
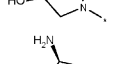
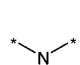
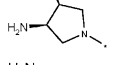
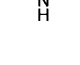
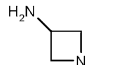
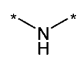
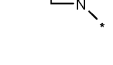











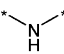
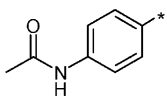
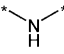
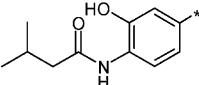
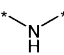
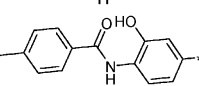
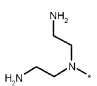
51*	A				2	---	8	5.097
52*	A				2	---	100	4
53	A				1	---	800	3.097
54*	A	H	TDA		2	---	16	4.796
55*	A	TDA	TDA		3	---	7	5.155
56	A	TDA	TDA		4	---	3	5.523
57*	A				2	---	10	5
58	A		TDA		3	---	18	4.745
59*	A				4	---	1	6
60	A		TDA		2	---	8	5.097
61	A				2	---	8	5.097
62*	A		TDA		3	---	11	4.959
63	A				4	---	1	6
64	A				2	---	10	5
65*	A		TDA		3	---	12	4.921
66*	A				4	---	13	4.886
67*	A				2	---	19	4.721
68*	A		TDA		3	---	13	4.886
69	A				4	---	15	4.824
70	A				2	---	10	5
71	A		TDA		3	---	19	4.721
72	A				4	---	21	4.678
73	A				2	---	17	4.769
74*	A		TDA		3	---	40	4.398
75	A				4	---	17	4.769
76	A				2	---	310	3.509
77	A		TDA		3	---	40	4.398
78*	A				4	---	44	4.356
79	A				2	---	21	4.678
80	A		TDA		3	---	31	4.509
81*	A				4	---	27	4.569
82*	A				2	---	72	4.143
83*	A		TDA		3	---	77	4.113
84	A				4	---	43	4.366
85*	A		TDA		3	---	58	4.236
86*	A				4	---	36	4.444
87*	A				3	---	14	4.854
88	A		TDA		4	---	11	4.959

Table 1 (Continued)

89	A	TDA	TDA			---	11	4.959
90*	A	TDA	TDA			---	12	4.921
91*	A	TDA	TDA			---	7	5.155
92*	A		TDA	NH ₂	---	---	10	5.000

Molecules indicated with * are included in test set.

be calculated at the grid points inside the molecules, not just outside, as it is in CoMFA [19].

All five physicochemical descriptors (electrostatic, steric, hydrophobic and H-bond donor and acceptor) were evaluated at each lattice interactions of a regularly spaced grid of 2.0 Å. A probe atom within radius of 1 Å, +1 charge, hydrophobicity +1.0 and H-bond donor and acceptor properties of +1.0 was used to evaluate steric, electrostatic, hydrophobic and H-bond donor and acceptor fields. Like in the CoMFA, the grid was extended beyond the molecular dimensions by 4.0 Å in *x*, *y* and *z* directions. For attenuation factor α controlling the steepness of Gaussian function the standard value of 0.3 was accepted.

2.5. Partial least square (PLS) analysis

Statistical analysis was performed by applying the partial least square (PLS) procedure to the appropriate columns of the CoMFA table and using the standard scaling method (CoMFA_STD). The cross-validation was performed using leave-one-out (LOO) method, wherein one compound is removed from the data set and its activity is predicted using the model derived from the rest of the data set. The cross-validated q^2 that resulted in optimum number of components (ONC) was considered. To speed up the analysis and to reduce noise, a minimum default column-filtering value (σ) of 2.00 kcal/mol (CoMFA) and 1.00 kcal/mol (CoMSIA) was used so that only those descriptor energies with values greater than the above described will be considered for PLS analysis. Final analysis (non-cross-validated) was performed to calculate conventional r^2 using the optimum number components obtained from the leave-one-out cross-validation analysis. To further assess the reliability, group cross-validation leave-five-out (LFO) with 10 groups and bootstrapping analysis were performed. After obtaining the models, the CoMFA, and CoMSIA results were graphically interpreted by field contribution maps. To obtain statistical confidence limits for the analyses statistics, bootstrapping [20,21] (10 runs) was performed at optimum *C* value in which the r^2 mean is given as q^2 bootstrap. Bootstrapping employs random sampling to pseudo-replicates of compounds from the original data set. A confidence measure by bootstrap validation is determined by

the standard deviation of the statistics obtained from bootstrapping.

2.6. Predictive correlation coefficient (r^2_{pred})

The predictive ability of the 3D-QSAR models was determined from a set of 37 compounds that were used as test set (Table 4). The predictive correlation coefficient (r^2_{pred}), based on test set molecules, is computed using

$$r^2_{\text{pred}} = \frac{\text{S.D.} - \text{PRESS}}{\text{S.D.}}$$

where S.D. is the sum of squared deviations between the biological activities of each molecule and the mean activity of the training set molecules and PRESS is the sum of squared deviations between the predicted and actual activity values for every molecule in the test set.

2.7. Docking studies

To predict the binding orientation of the highly active compound inside the major groove of RNA and also to study the interactions between the ligand and receptor, docking studies were performed using Autodock version 3.0. AutoDock is a fully automated docking suite of programs, which employs a Lamarckian genetic algorithm (LGA) as a search engine (50 LGA runs) and a LUDI-type scoring function. The number of individuals in each population was set at 80. The maximum number of energy evaluations was set at 900,000 and the maximum number of generations was set at 50,000. The number of top docking orientations that automatically appear during the calculations was fixed at two. The rates of gene mutation and crossover were set at 0.02 and 0.80, respectively. We have found that these settings give consistent results in the distribution of the final top 50 structures. During this searching process, the ligands (i.e. substrates) were regarded as being flexible, while the enzyme was regarded as rigid and each of its atoms was approximated as a grid point.

The grids were prepared using the autogrid facility provided with the AutoDock package. All the energy scoring grids have the same size (60 × 60 × 60 points, spacing 0.375 Å) and the

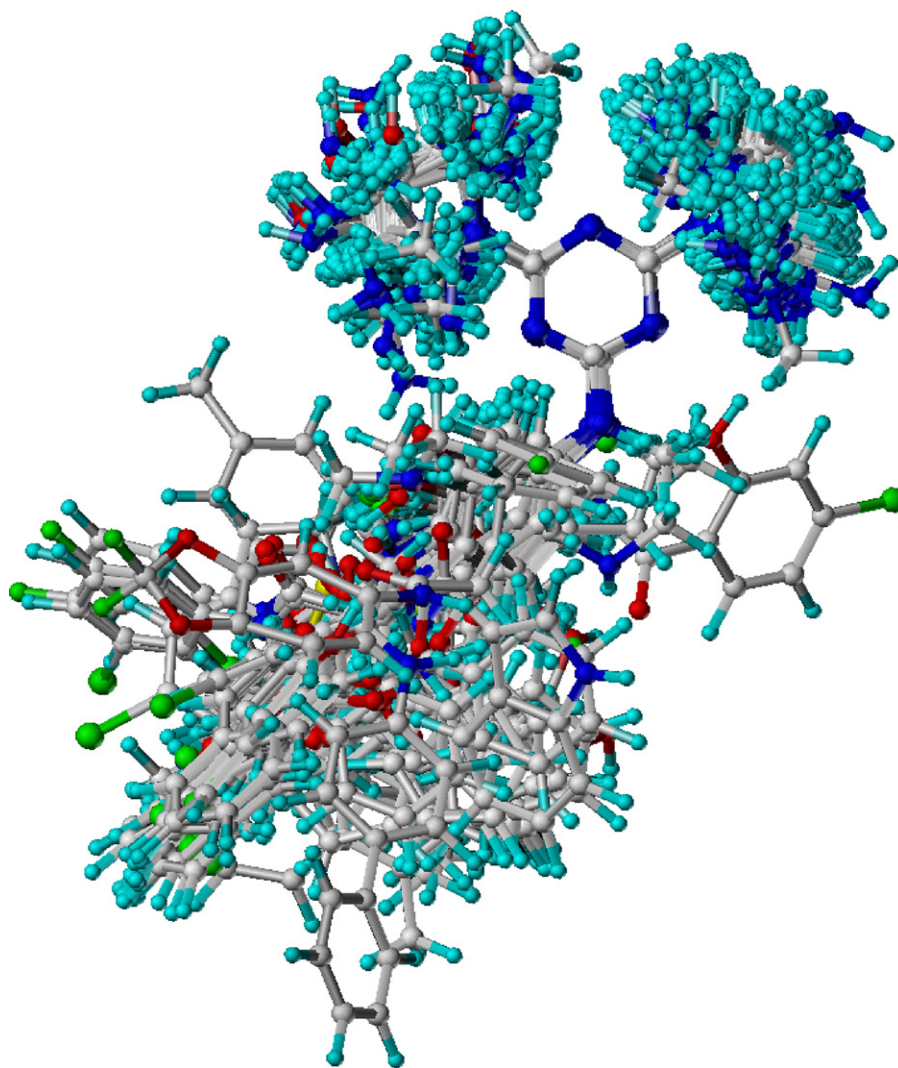


Fig. 2. 3D-view of aligned molecules (training and test sets) based on rms fit alignment method.

same position in space. The RNA oligomers and ligands were charged according to AMBER [22,23] charges and Gasteiger-Marsilli charges [17], respectively. According to Detering and Varani, a charge of +1 was added to each phosphorus atom to neutralize the systems.

3. Results and discussion

3.1. 3D-QSAR studies

A data set of 55 TDA derivatives having antibacterial translation inhibitory activities was used to derive both the conventional CoMFA and CoMSIA models. An external test set of 37 compounds with chemical diversity and having all ranges of activity was used to determine the accuracy of the models.

3.1.1. CoMFA analysis

The leave-one-out partial least-squares (PLS) analysis of the obtained models yielded excellent cross-validated q^2 -values of 0.708 with five components. As cross-validated correlation

coefficient (q^2) is used as a measure of reliability of prediction, these correlation coefficients suggest that our model is reliable and accurate. Subsequently, internal non-cross-validated PLS regressions were computed using the previously obtained optimum number of components giving regression coefficients r^2 of 0.967 with a standard error of estimate (SEE) of 0.099. The conventional correlation coefficient indicates the goodness of the fit of QSAR model. The statistical parameters associated with all models are shown in Table 2.

The predicted pIC_{50} values and residual values for training and test set compounds are given in Tables 3 and 4, respectively. Fig. 3 shows the relationship between the CoMFA-predicted and experimental pIC_{50} values of the non-cross-validated analyses for TDA derivatives.

3.1.2. CoMSIA analysis

CoMSIA is an alternative molecular field analysis method to CoMFA. It is thought to be less affected by changes in molecular alignment and to provide more smooth and interpretable contour maps as a result of employing Gaussian

Table 2
Summary of CoMFA and CoMSIA results

QSAR parameters	CoMFA	CoMSIA
q^2_{LOO}	0.708	0.556
q^2_{LFO}	0.733	0.593
r^2	0.967	0.935
ONC	5	6
SEE	0.099	0.140
F-value	287.737	115.782
r^2_{bs}	0.969	0.966
S.D.	0.007	0.012
r^2_{pred}	0.632	0.653
Fraction of field contribution		
Steric	0.438	0.141
Electrostatic	0.562	0.236
Hydrophobic	–	0.219
Acceptor	–	0.220
Donor	–	0.183

q^2_{LOO} , Cross-validated correlation with leave-one-out; ONC, optimum number of components as determined by LOO study; SEE, standard error of estimation; q^2_{LFO} , group cross-validation coefficient for leave-five-out; r^2_{pred} , predictive correlation coefficient; r^2_{bs} , correlation coefficient after 10 runs of bootstrapping; S.D., standard deviation for 10 runs of bootstrapping.

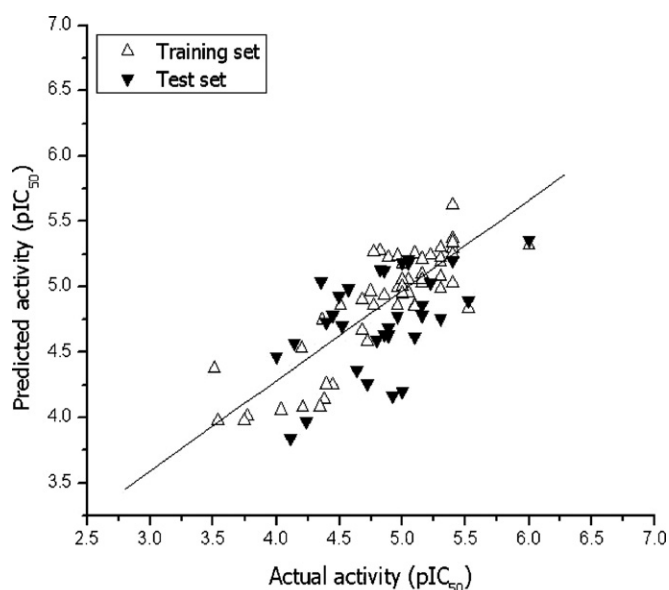


Fig. 3. Experimental activities vs. predicted activities for compounds in the training and test sets using CoMFA model.

type distance dependence with the molecular similarity indices it uses [24]. CoMSIA models were generated using the combinations of the following descriptor fields: steric, electrostatic, hydrophobic, H-bond donor and H-bond acceptor. These descriptors illustrate the various properties into spatial locations where they play a decisive role in determining the biological activity. The statistical details of CoMSIA model are summarized in Table 2. A combined use of all the five descriptors resulted in the best model (q^2 0.556 and (r^2 0.935 with six components). Although the q^2 values of the CoMSIA models reduced compared to those of the CoMFA models, they are still indicating stable analyses of high quality. Final

Table 3
Experimental and predicted biological activities and residuals obtained by the CoMFA and CoMSIA models for training set compounds

Comp.	Activity ^a	CoMFA		CoMSIA	
		Predicted	Residual	Predicted	Residual
1	4.377	4.137	0.240	4.008	0.369
2	4.036	4.058	−0.022	3.924	0.112
3	4.347	4.084	0.263	4.008	0.339
4	4.208	4.076	0.132	4.338	−0.13
5	3.769	4.013	−0.244	4.370	−0.601
6	3.538	3.978	−0.440	3.980	−0.442
7	3.745	3.979	−0.234	3.939	−0.194
8	4.201	4.529	−0.328	4.753	−0.552
10	4.444	4.253	0.191	4.161	0.283
12	5.046	4.955	0.091	4.944	0.102
13	5.155	5.097	0.058	4.943	0.212
14	5.097	4.860	0.237	4.866	0.231
15	5.398	5.294	0.104	4.412	0.986
16	5.398	5.291	0.107	5.161	0.237
19	5.301	5.192	0.109	5.215	0.086
20	5.398	5.629	−0.231	5.914	−0.516
21	4.886	5.227	−0.341	5.217	−0.331
23	4.959	5.237	−0.278	5.343	−0.384
25	4.959	4.997	−0.038	4.749	0.210
26	5.097	5.254	−0.157	4.944	0.153
28	5.301	5.081	0.220	5.324	−0.023
30	5.046	5.055	−0.009	5.041	0.005
31	5.156	5.029	0.127	5.035	0.121
32	5.000	5.171	−0.171	5.251	−0.251
33	4.854	4.931	−0.077	4.962	−0.108
34	5.398	5.372	0.026	5.122	0.276
35	5.301	4.984	0.317	4.863	0.438
38	5.398	5.250	0.148	5.162	0.236
39	5.398	5.026	0.372	5.165	0.233
40	5.222	5.243	−0.021	5.086	0.136
41	5.398	5.339	0.059	5.301	0.097
44	5.301	5.22	0.081	5.419	−0.118
45	5.000	5.056	−0.056	4.734	0.266
46	5.155	5.211	−0.056	4.988	0.167
47	5.000	4.941	0.059	4.890	0.110
49	5.155	5.05	0.105	4.989	0.166
50	5.301	5.302	−0.001	5.180	0.121
56	5.523	4.830	0.693	5.462	0.061
58	4.745	4.963	−0.218	4.655	0.090
60	5.097	4.846	0.251	4.872	0.225
61	5.097	4.845	0.252	5.401	−0.304
63	6.000	5.315	0.685	5.138	0.862
64	5.000	5.005	−0.005	4.926	0.074
69	4.824	5.277	−0.453	5.030	−0.206
70	5.000	4.950	0.050	4.735	0.265
71	4.721	4.582	0.139	4.617	0.104
72	4.678	4.666	0.012	5.099	−0.421
73	4.769	4.859	−0.090	4.356	0.413
75	4.769	5.267	−0.498	5.272	−0.503
76	3.509	4.374	−0.865	4.606	−1.097
77	4.398	4.255	0.143	3.941	0.457
79	4.678	4.901	−0.223	4.498	0.180
80	4.509	4.856	−0.347	5.084	−0.575
84	4.366	4.747	−0.381	4.447	−0.081
88	4.959	4.860	0.099	4.452	0.507

^a The experimental activities expressed in pIC_{50} ($-\log IC_{50}$).

predicted/cross-validated versus experimental pIC_{50} values for models and their residuals are given in Tables 3 and 4. Fig. 4 shows the experimental activities versus predicted ones in the training and test sets by CoMSIA models.

Table 4

Experimental and predicted biological activities and residuals obtained by the CoMFA and CoMSIA models for test set compounds

Comp.	Activity ^a	CoMFA		CoMSIA	
		Predicted	Residual	Predicted	Residual
9	4.638	4.364	0.274	3.979	0.659
11	4.495	4.926	−0.431	5.052	−0.557
17	5.523	4.893	0.630	4.894	0.629
18	5.301	4.756	0.545	4.587	0.714
22	4.824	5.131	−0.307	5.131	−0.307
24	4.854	5.123	−0.269	5.148	−0.294
27	4.523	4.707	−0.184	4.717	−0.194
29	5.398	5.203	0.195	4.963	0.435
36	5.046	5.184	−0.138	5.368	−0.322
37	5.000	5.182	−0.182	5.225	−0.225
42	5.046	5.21	−0.164	5.381	−0.335
43	5.222	5.033	0.189	4.916	0.306
48	5.155	4.859	0.296	5.063	0.092
51	5.097	4.618	0.479	4.312	0.785
52	4.000	4.465	−0.465	4.382	−0.382
53	3.097	3.648	−0.551	3.533	−0.436
54	4.796	4.593	0.203	4.424	0.372
55	5.155	4.786	0.369	5.014	0.141
57	5.000	4.202	0.798	4.647	0.353
59	6.000	5.352	0.648	5.318	0.682
62	4.959	4.775	0.184	5.237	−0.278
65	4.921	4.17	0.751	4.464	0.457
66	4.886	4.633	0.253	4.983	−0.097
67	4.721	4.259	0.462	4.023	0.698
68	4.886	4.691	0.195	4.370	0.516
74	4.398	4.733	−0.335	4.706	−0.308
78	4.356	5.042	−0.686	4.841	−0.485
81	4.569	4.984	−0.415	4.765	−0.196
82	4.143	4.572	−0.429	4.256	−0.113
83	4.113	3.84	0.273	3.870	0.243
85	4.236	3.97	0.266	4.158	0.078
86	4.444	4.779	−0.335	4.783	−0.339
87	4.854	4.641	0.213	4.326	0.528
89	4.959	4.891	0.068	5.111	−0.152
90	4.921	5.009	−0.088	5.016	−0.095
91	5.155	5.276	−0.121	5.316	−0.161
92	5.000	4.379	0.621	4.253	0.747

^a The experimental activities expressed in pIC_{50} ($-\log IC_{50}$).

3.1.3. Validation of QSAR models

The validation of QSAR models was done to verify the excellent statistical parameters that were observed and also to investigate whether 1,3,5-triazine-2,4-diamines can be predicted well with is model, which are reproduced the experimental activity very well for the training set. A large data set of compounds containing 37 molecules, as a test set (Table 4) was selected for the original data of 92 compounds for the validation experiments. The ultimate test for the predictability of a QSAR analysis in the drug design process is to predict the biological activity of new compounds that have not been included in the training set. The predicted versus the experimental selectivity values for the training and test sets are depicted in Figs. 3 and 4. The value of r^2_{pred} was calculated for the test set according to the formula of Cramer et al. [21] and gave better results for CoMSIA, with the value of 0.653 than for the CoMFA model 0.632. Thus, our models display very high predictivity both in regular cross-validation and in the prediction of a test set.

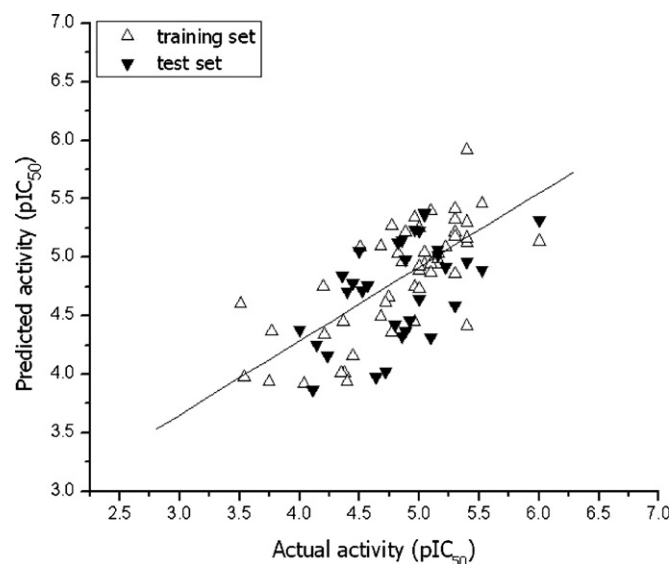


Fig. 4. Experimental activities vs. predicted activities for compounds in the training and test sets using CoMSIA models.

3.1.4. CoMFA and CoMSIA contours maps

To visualize the information content of the derived 3D-QSAR models, CoMFA and CoMSIA contour maps were generated. The field energies at each lattice point were calculated as the scalar results of the coefficient and the standard deviation associated with a particular column of the data table (“S.D.*coeff”), which was always plotted as the percentage of the contribution to the CoMFA or CoMSIA equation. In the figures, the isocontour diagrams of the field contributions (“S.D.*coeff”) for different properties calculated by the CoMFA and CoMSIA analysis are illustrated with exemplary ligands. Selectivity fields depict the change in binding preference occurring upon the change in molecular fields around ligands. The contour plots may help to identify important regions where any change may affect the binding preference. Furthermore, they may be helpful in identifying important features contributing to interactions between the ligand and the active site of a receptor. For the CoMFA steric, electrostatic fields and CoMSIA steric, electrostatic, acceptor, donor and hydrophobic fields, the contours represent 80% and 20% level contributions. For convenience, all similar contour map positions were labeled and shown in contribution with the highly active compound **63**. As depicted from Figs. 5 and 6(A), the big green contours around triazine’s 4 and 6 substituents, indicate that steric bulk is favored for activity in these areas. This may be the reason why compounds with large aromatic substituents in this area, e.g. compounds **29**, **34**, **38–41**, **48**, **56**, **59** and **63** are more potent than molecules with small substituents, such as compounds **11**, **21–25** and **53**. The decreased activity of compound **54**, due to H atom substitution at C⁶ and the lack of aromatic substitutions near C⁴ in compounds **6** and **7** proved the importance of above described groups. There is one yellow contour map labeled 2 in Fig. 5A, which indicates that steric bulk is disfavored for activity in this area. For example, the order of compounds **9** > **10** > **4** > **8** > **7** > **6** shows the addition of steric bulky groups, such as methyl and ethyl groups cause detrimental effect

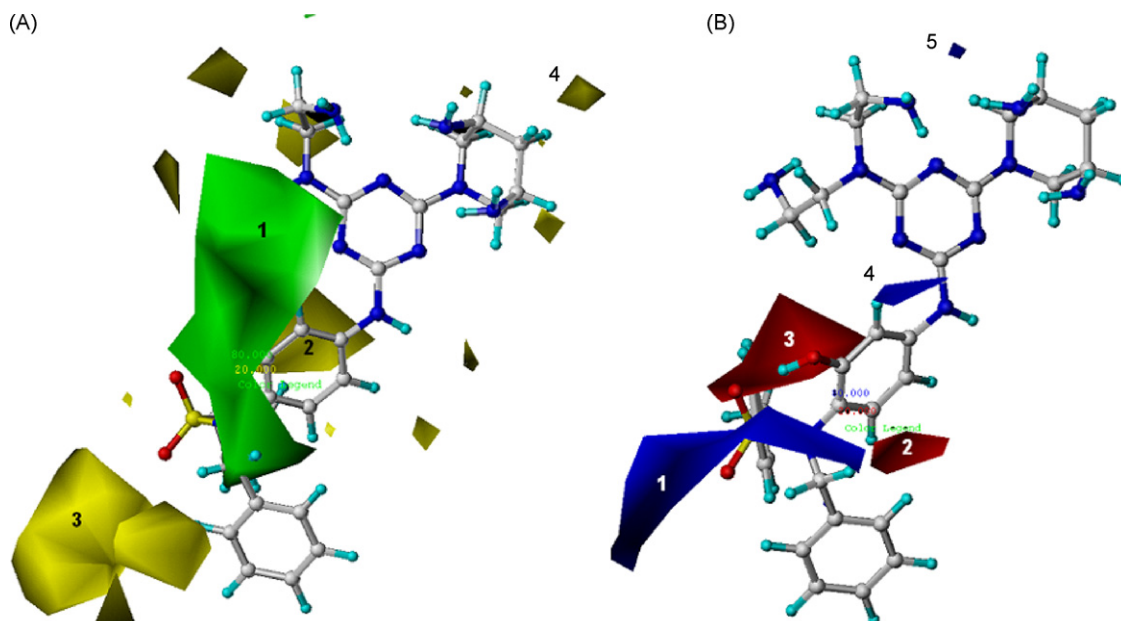


Fig. 5. CoMFA S.D.* coeff contour maps illustrating steric and electrostatic features in combination with compound **63**. (A) The green contour for steric favored region and yellow maps calls for a reduction of this potential to improve affinity. (B) Blue for positive charge preferred region to improve binding affinity.

on biological activity of compounds. Two yellow contour maps exist towards the C² and C⁶ positions, labeled 4. The pyrrolidine substitution in these areas proves the loss of activity in compounds **64–69**, **82–86**. Also, azetidine substitution in this area yields moderately active analogs **87**, **88**. Two more yellow contour maps present labeled as 3 in Fig. 5A, which disfavors bulky groups in this region. This can be explained by the fact that the compounds with substitution 4 are highly active compare to the 2 and 3 side groups (Table 1). The CoMFA electrostatic contour plots are displayed in Fig. 5B. The blue contour map

(labeled 1) between the phenyl and benzyl groups indicates that any positive charge or electron deficient substitute will enhance the activity at this position. For example, the compound **63**, which contains electro positive group, shows highest activity and compound **53** having no such group exhibits lowest activity. Two red contour maps obtained above and below of phenyl ring illustrates that negative charged group is favored in these areas. The hydroxyl and halogen groups of compounds **17**, **18**, **19**, **34**, **38**, **39**, **44**, **56**, **59**, **63**, projected toward these contours and were showing good activity. The two small blue contours (labeled 4

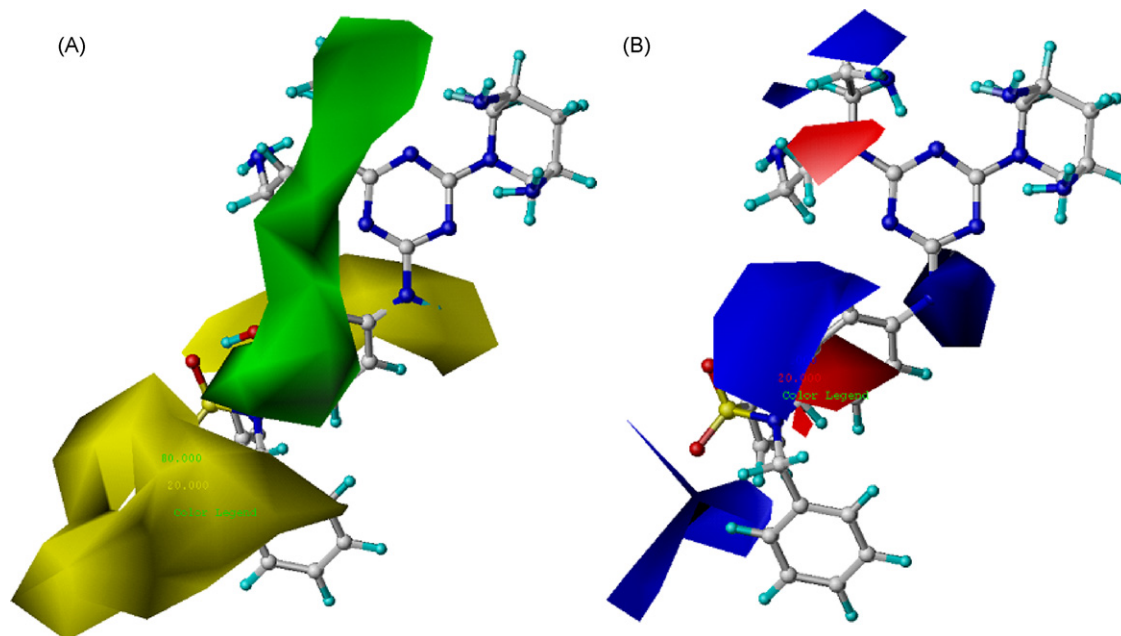


Fig. 6. CoMSIA S.D.* coeff contour maps illustrating steric and electrostatic features in combination with compound **63**. (A) The green contour for steric favored region and yellow maps calls for a reduction of this potential to improve affinity. (B) Blue for positive charge preferred region to improve binding affinity.

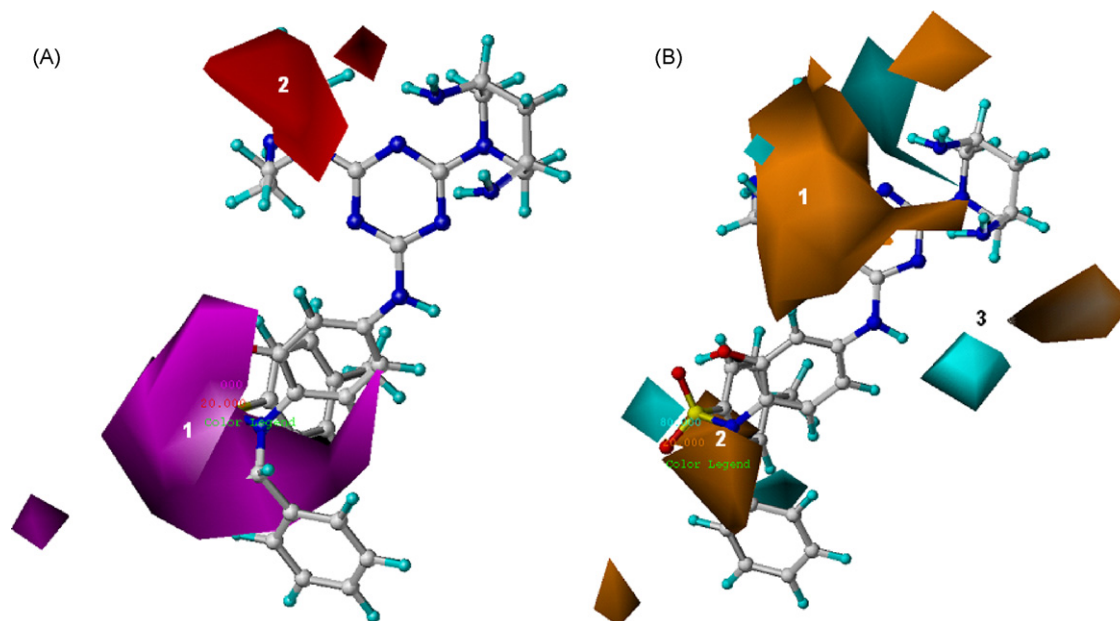


Fig. 7. CoMSIA S.D.* coeff contour maps illustrating acceptor and donor features in combination with compound **63**. (A) The magenta contour for H-bond acceptor group increase activity, red indicates the disfavor region. (B) The cyan contour for H-bond donor favor region, orange indicates the disfavor region.

and 5) near the C⁴ and C⁶ of triazine ring indicates that the electron deficient substituents increase the activity. The amino group of the compounds **5** and **60** pointed towards this blue contour present near C⁶ position and showing higher activity than the compounds **52** and **76** which contains OH group.

Fig. 6A and B describe the steric and electrostatic contour maps of the CoMSIA models. These contours are almost similar to the CoMFA-steric and electrostatic contours (Fig. 5A and B). But in CoMSIA model, two more contours appeared: the blue contour mapped on the phenyl ring and a red contour map near the electron rich tertiary nitrogen of *N,N*-bis (aminomethyl) amine substituted at C⁶ position of triazine ring. In Fig. 7A, the big magenta contour (labeled 1) surrounding the phenyl ring, indicates the presence of any substituents contain acceptor group increases the activity. The carbonyl groups of the compounds **26**, **38** and **40–46**, and were showing good activity. The small red contours (labeled 2) in Fig. 6A, indicates that the substituents with hydrogen-bond acceptors are unfavored in these areas. The oxygen of hydroxyl group of the compounds **52**, **67**, **73**, **76** and **82** are buried in this contour and having less activity. The hydrogen-bond donor contours of Fig. 7B are signifying the regions of hydrogen-bond donor favorable (cyan) and unfavorable (orange) regions. The three cyan contours are mapped near the hydroxyl, NH and NH₂ groups of compound **59** (Fig. 7B) and signifies the position of donor groups present in the anti-bacterial compounds. In Fig. 8, the yellow and white contours enclose regions favorable for hydrophobic and hydrophilic groups, respectively. The yellow contour labeled 1 in Fig. 8 support the importance of aromatic ring substitutions at R4 position as shown in scaffold A. The methyl group in compounds **50** and **60** satisfies another small yellow contour map (labeled 3). The amino groups exhibit the perfect fit to all the white contours.

3.2. Docking studies

Initially, the docking reliability was validated using the known X-ray structure of dry RNA (without water) in complex with a small molecular ligand paromomycin (1J7T) [25] using

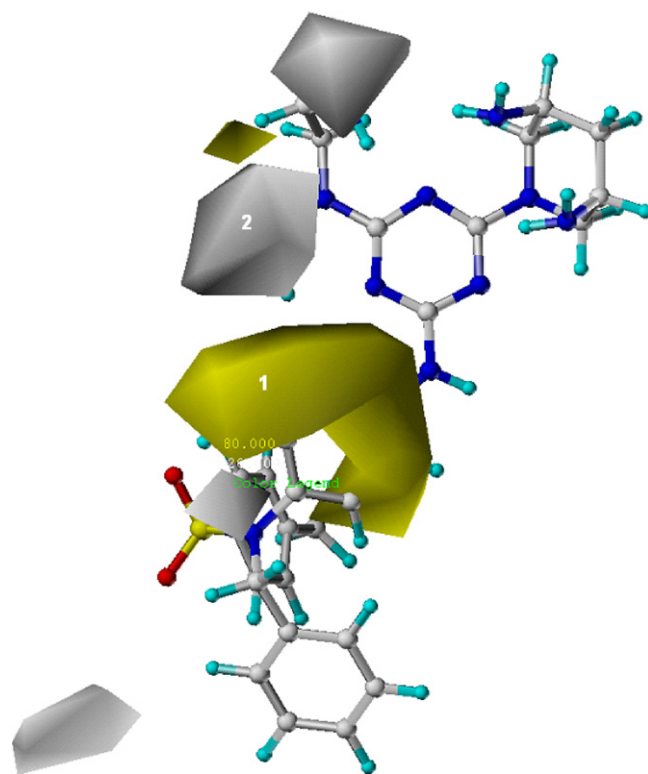


Fig. 8. CoMSIA S.D.* coeff contour maps illustrating hydrophobic features in combination with compound **63**. The yellow contour for hydrophobic favor region, white indicates the hydrophilic favored region.

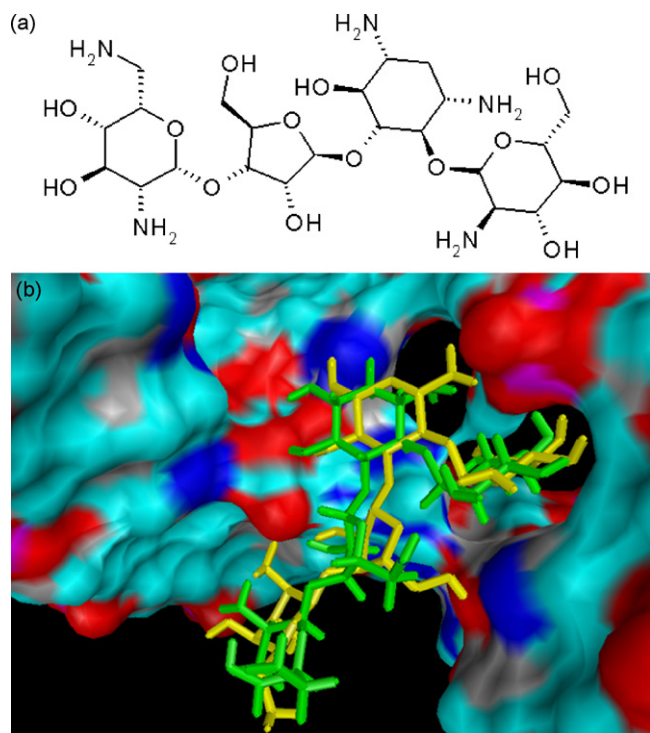


Fig. 9. (a) Structure of paromomycin and (b) comparison of paromomycin experimental binding mode (green) and docking pose (yellow) with lowest RMSD.

AutoDock v3.0. [26]. The ligand paromomycin was re-docked to the major groove of dry RNA and the docked conformation corresponding to the lowest free energies was selected as the most probable binding conformation. The root mean-square deviation (RMSD) between the crystal ligand and the docked conformation is equal to 2.95 Å and it results in a poor docking accuracy. Several attempts have been made to increase the docking accuracy by adding water molecules [27–30]. The water molecules participate to some key drug/RNA interactions. Crystallographic water molecules, present the crystal structure was now be considered in the docking process. This process generated the conformation with lowest RMSD of 1.67 Å (Fig. 9). This method was used for the docking of the best molecule (compound **63**) present in the TDA derivatives into the major groove of RNA.

Figs. 10 and 11 shows the binding orientation of compound **63** in the binding site of RNA. The electron rich N⁵ of triazine ring present in the compound **63** is having hydrogen bond with NH of Adenine21. The N¹ of the compound is interacting with RNA (A17) through the bridge water molecule and signifying the importance of water in ligand binding. The two di-amino groups located on either side of the triazine ring are forming a network of hydrogen bonds with RNA (A21, C28, G18, A16 and G15). This was indicated by electro positive (blue) contour in the CoMFA electrostatic map (Fig. 5B) and as donor favorable (orange) contour (Fig. 7B) in CoMSIA. The bridge

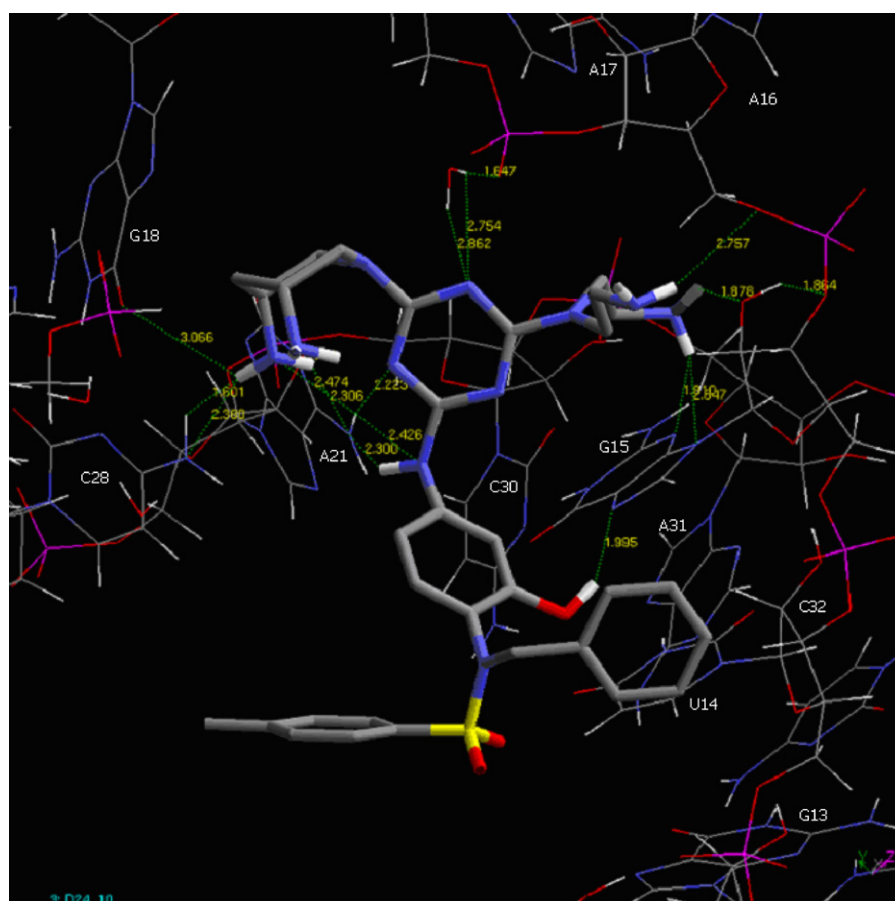


Fig. 10. Docked conformation of compound **63** inside the major groove of rRNA. Yellow dotted lines represent the hydrogen bonds.

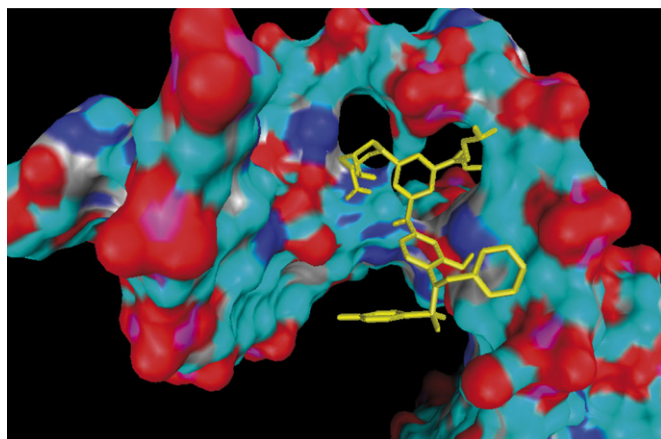


Fig. 11. Docked pose of compound **63** in rRNA molecular surface.

amine group, in C4, between triazine and phenyl ring is showing hydrogen-bond interactions with NH of Adenine 21. It appeared as blue contour in CoMFA and CoMSIA electrostatic maps and orange contour in CoMSIA donor maps. The hydroxyl group of the compound **63** is forming hydrogen bond with electron rich nitrogen of G15.

4. Summary

The present studies were aimed at deriving predictive models capable of elucidating the structural requirements for antibacterial translation inhibitors. The 3D-QSAR analyses of 1,3,5-triazine-2,4-diamine derivatives as antibacterial translation inhibitors were carried out using CoMFA and CoMSIA methods. The CoMFA and CoMSIA models provided similar results and both are having dominant electrostatic interactions. It is evident from the contour maps of CoMFA and CoMSIA that the electrostatic effects determine the binding affinity. The relative contributions of electronic fields are larger than steric fields in both CoMFA and CoMSIA. The effects of the steric, electrostatic, hydrophobic and H-bond donor and acceptor fields around the docked conformations on their activities were discussed in detail. According to these studies, some implications could be drawn to improve the activity and selectivity of piperidinyl triazines as bacterial translation inhibitors, for example, requirement of amino aromatic groups with a subtle balance of both electropositive and electronegative groups at C⁴ position to improve activity. Presence of amino substitutions in the vicinity of the positions 3 and 5 of the diamino piperidinyl triazine, improves biological activity. Further, the docking studies were performed to explore the probable binding conformation inside the binding site of RNA. It is evident that the network of hydrogen bonds formed between RNA and the ligand are crucial for molecular recognition.

The obtained models will serve as a basis for the design of novel antibacterial compounds with enhanced activity and other tailored properties. The information on the receptor binding sites also provides an opportunity for the design of specific probes to be used in studies seeking to elucidate the mechanism of action of these drug molecules.

Acknowledgements

We are thankful to the management of PGRRCDE, Osmania University for providing the adequate facilities, Dr. J.A.R.P. Sarma, Director, and Dr. Kishore M., Informatics Division, GVK Biosciences Pvt. Ltd., for providing software facilities and giving a great chance to work there.

References

- [1] N. Woodford, Novel agents for the treatment of resistant Gram-positive infections, *Exp. Opin. Investig. Drugs* 12 (2003) 117–137.
- [2] M. Khare, D. Keady, Antimicrobial therapy of methicillin resistant *Staphylococcus aureus* infection, *Exp. Opin. Pharmacother.* 4 (2003) 165–177.
- [3] J.M. Hamilton-Miller, Vancomycin-Resistant, *Staphylococcus aureus*: a real and present danger? *Infection* 30 (2002) 118–124.
- [4] L.B. Rice, Antimicrobial resistance in Gram-positive bacteria, *Am. J. Infect. Control* 34 (2006) S11–S19.
- [5] S. Tsiodras, H.S. Gold, G. Sakoulas, et al., Linezolid resistance in a clinical isolate of *Staphylococcus aureus*, *Lancet* 358 (2001) 207–208.
- [6] P.K. Lakshmi, J. Haddad, S. Mobashery, Aminoglycosides: perspectives on mechanisms of action and resistance and strategies to counter resistance, *Antimicrob. Agents Chemother.* 44 (2000) 3249–3256.
- [7] F. Franceschi, E.M. Duffy, Structure-based drug design meets the ribosome, *Biochem. Pharmacol.* 71 (2006) 1016–1025.
- [8] J. Poehlsgaard, S. Douthwaite, The bacterial ribosome as a target for antibiotics, *Nat. Rev. Microbiol.* 3 (2005) 870–881.
- [9] T. Tenson, A. Mankin, Antibiotics and the ribosome, *Mol. Microbiol.* 59 (2006) 1664–1677.
- [10] Y. Zhou, Z. Sun, V.E. Gregor, et al., Structure-guided discovery of novel aminoglycoside mimetics as antibacterial translation inhibitors, *Antimicrob. Agents Chemother.* 49 (2005) 4942–4949.
- [11] Y. Zhou, Z. Sun, J.M. Froelich, et al., Structure-activity relationships of novel antibacterial translation inhibitors: 3,5-diamino-piperidinyl triazines, *Bioorg. Med. Chem. Lett.* 16 (2006) 5451–5456.
- [12] Y. Zhou, V.E. Gregor, B.K. Ayida, et al., Synthesis SAR of 3,5-diamino-piperidine derivatives: novel antibacterial translation inhibitors as aminoglycoside mimetics, *Bioorg. Med. Chem. Lett.* 17 (2007) 1206–1210.
- [13] R.D. Cramer III, D.E. Patterson, J.D. Bunce, Comparative molecular field analysis (CoMFA). 1. Effect of shape on binding of steroids to carrier proteins, *J. Am. Chem. Soc.* 110 (1988) 5959–5967.
- [14] M. Bohm, J. Sturzebecher, G. Klebe, Three-dimensional quantitative structure-activity relationship analyses using comparative molecular field analysis and comparative molecular similarity indices analysis to elucidate selectivity differences of inhibitors binding to trypsin, thrombin, and factor Xa, *J. Med. Chem.* 42 (1999) 458–477.
- [15] Sybyl 6.8.1, Tripos Inc., 1699 South Hanley Road, St. Louis, MO 63144, U.S.A.
- [16] M. Clark, R.D. Cramer III, N. Van Opdenbosch, Validation of the general purpose Tripos 5.2 force field, *J. Comput. Chem.* 10 (1989) 982–1012.
- [17] J. Gasteiger, M. Marsili, Iterative partial equalization of orbital. Electronegativity—a rapid access to atomic charges, *Tetrahedron* 36 (1980) 3219–3228.
- [18] J.J.P. Stewart, MOPAC: a semiempirical molecular orbital program, *J. Comput. Aided Mol. Des.* 4 (1990) 1–103.
- [19] H. Kubinyi (Ed.), 3D-QSAR in Drug Design. Theory, Methods and Applications, ESCOM, Leiden, The Netherlands, 1993, pp. 443–485.
- [20] L. Stahle, S. Wold, Multivariate data analysis and experimental design in biomedical research, *Prog. Med. Chem.* 25 (1988) 292–338.
- [21] R.D. Cramer III, J.D. Bunce, D.E. Patterson, I.E. Frank, Crossvalidation, bootstrapping, and partial least squares compared with multiple regression in conventional QSAR studies, *Quant. Struct. Act. Relat.* 7 (1988) 18–25.
- [22] S.J. Weiner, P.A. Kollman, D.A. Case, et al., New force field for molecular mechanical simulation of nucleic acids and proteins, *J. Am. Chem. Soc.* 106 (1984) 765–784.

- [23] S.J. Weiner, P.A. Kollman, D.T. Nguyen, D.A. Case, An all atom force field for simulations of proteins and nucleic acids, *J. Comput. Chem.* 7 (1986) 230–252.
- [24] G. Kliebe, U. Abraham, T. Mietzner, Molecular similarity indices in a comparative analysis (CoMSIA) of drug molecules to correlate and predict their biological activity, *J. Med. Chem.* 37 (1994) 4130–4146.
- [25] <http://www.rcsb.org/pdb/1J7T>.
- [26] G.M. Morris, S.G. David, S.H. Robert, H. Ruth, E.H. William, K.B. Richard, J.O. Arthur, Automated docking using a Lamarckian genetic algorithm and an empirical binding free energy function, *J. Comp. Chem.* 19 (1998) 1639–1662.
- [27] M.L. Verdonk, G. Chessari, J.C. Cole, M.J. Hartshorn, C.W. Murray, J.W.M. Nissink, R.D. Taylor, R. Taylor, Modeling water molecules in protein-ligand docking using GOLD, *J. Med. Chem.* 48 (2005) 6504–6515.
- [28] C. de Graaf, P. Pospisil, W. Pos, G. Folkers, N.P.E. Vermeulen, Binding mode prediction of cytochrome P450 and thymidine kinase protein-ligand complexes by consideration of water and rescoring in automated docking, *J. Med. Chem.* 48 (2005) 2308–2318.
- [29] M. Fornabaio, F. Spyraakis, A. Mozzarelli, P. Cozzini, D.J. Abraham, G.E. Kellogg, Simple, intuitive calculations of free energy of binding for protein-ligand complexes. 3. The free energy contribution of structural water molecules in HIV-1 protease complexes, *J. Med. Chem.* 47 (2004) 4507–4516.
- [30] N. Moitessier, E. Westhof, S. Hanessian, Docking of aminoglycosides to hydrated and flexible RNA, *J. Med. Chem.* 49 (2006) 1023–1033.